ACSNANO

www.acsnano.org

ARTICLE

Ultrasmall Folate Receptor Alpha Targeted Enzymatically Cleavable Silica Nanoparticle Drug Conjugates Augment Penetration and Therapeutic Efficacy in Models of Cancer

Fei Wu,[#] Pei-Ming Chen,[#] Thomas C. Gardinier, Melik Z. Turker, Aranapakam M. Venkatesan, Vaibhav Patel, Tin Khor, Michelle S. Bradbury, Ulrich B. Wiesner, Gregory P. Adams, Geno Germano, Feng Chen,[*,▽] and Kai Ma[*,▽]

Cite This: https://doi.org/10.1021/acsnano.2c05342 Read Online

ACCESS | Metrics & More | Article Recommendations | Supporting Information

ABSTRACT: To address the key challenges in the development of next-generation drug delivery systems (DDS) with desired physicochemical properties to overcome limitations regarding safety, in vivo efficacy, and solid tumor penetration, an ultrasmall folate receptor alpha (FRα) targeted silica nanoparticle (C'Dot) drug conjugate (CDC; or folic acid CDC) was developed. A broad array of methods was employed to screen a panel of CDCs and identify a lead folic acid CDC for clinical development. These included comparing the performance against antibody−drug conjugates (ADCs) in three-dimensional tumor spheroid penetration ability, assessing in vitro/ex vivo cytotoxic efficacy, as well as in vivo therapeutic outcome in multiple cell-line-derived and patient-derived xenograft models. An ultrasmall folic acid CDC, EC112002, was identified as the lead candidate out of >500 folic acid CDC formulations evaluated. Systematic studies demonstrated that the lead formulation, EC112002, exhibited highly specific FRα targeting, multivalent binding properties that would mediate the ability to outcompete endogenous folate *in vivo*, enzymatic responsive payload cleavage, stability in human plasma, rapid *in vivo* clearance, and minimal normal organ retention organ distribution in non-tumor-bearing mice. When compared with an anti-FRα-DM4 ADC, EC112002 demonstrated deeper penetration into 3D cell-line-derived tumor spheroids and superior specific cytotoxicity in a panel of 3D patient-derived tumor spheroids, as well as enhanced efficacy in cell-line-derived and patient-derived *in vivo* tumor xenograft models expressing a range of low to high levels of FRα. With the growing interest in developing clinically translatable, safe, and efficacious DDSs, EC112002 has the potential to address some of the critical limitations of the current systemic drug delivery for cancer management.

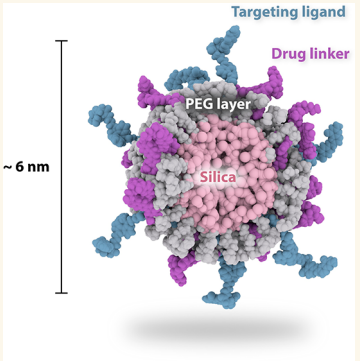

KEYWORDS: *ultrasmall, folate receptor alpha, silica nanoparticle drug conjugates, patient-derived ovarian cancer, tumor spheroids, penetration*

INTRODUCTION

Inefficient and imprecise delivery of chemotherapeutic drugs to cancer cells is one of the key contributions to the unwanted side effects, drug resistance and overall low survival rates of cancer patients.[1] To date, liposomes and antibodies are the two main carriers that have been approved by the United States Food and Drug Administration (FDA) for improving the toxic payload delivery efficiency in cancer patient care via systemic administration.[2,3] While eight liposomal drugs have been approved for cancer management with improved biodistribution and reduced toxicity as compared to drug-alone formulations,[2] they all rely on enhanced permeability and retention (EPR) effects in patients with limited solid tumor penetration due to their large vehicle size.[4,5] On the other hand, antibody−drug conjugates (ADCs) have shown considerable success in treating both hematologic and solid tumors, with a total of 12 ADCs approved in the past two decades (Table S1).[3] However, challenges still remain for

Received: May 31, 2022
Accepted: October 14, 2022

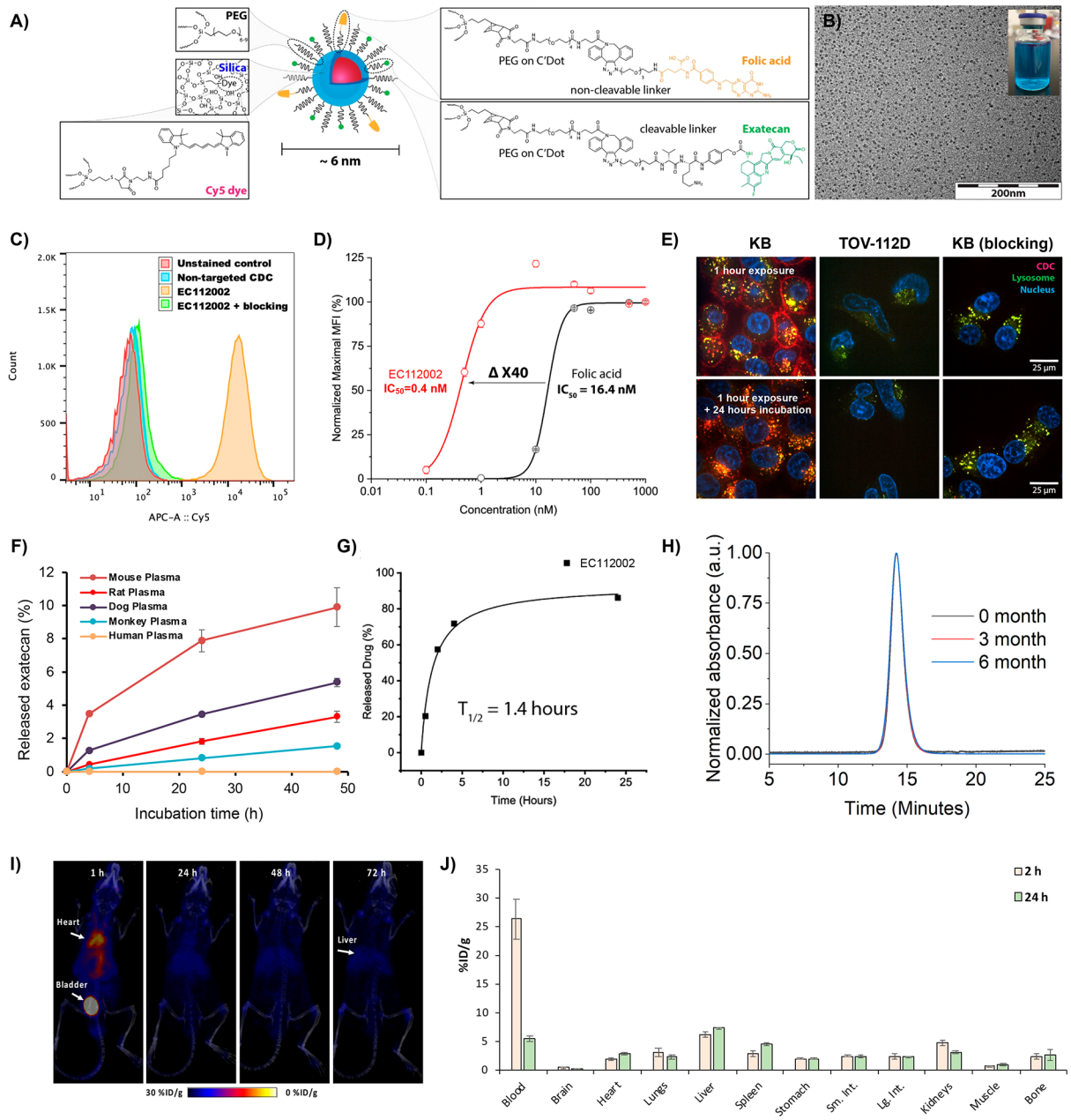

Figure 1. Design and characterizations of EC112002. (A) A schematic illustration of key components of EC112002 folic acid CDC. (B) A representative TEM image of EC112002. Scale bar: 200 nm. Inset: Photo of EC112002 in the container-enclosure system showing its characteristic blue color as a result of encapsulated Cy5 dye. (C) Flow cytometry of EC112002, nontargeted control nanoparticle (with a similar number of payloads but no folic acid ligands) in human KB (FRα positive). The blocking group used the same EC112002 along with 1 mM of free folic acid. (D) A competitive binding study between EC112002 and free folic acid showed the multivalency effect of EC112002. Increasing concentrations of EC112002 or free folic acid were selected to compete off the green-dye-conjugated folic acid molecules (10 nM) that previously bound to the KB cells. (E) Confocal microscopy images of EC112002 in human KB (FRα positive) and TOV-112D (FRα negative) cell lines. Top panel: 1-h exposure group. Bottom panel: 1-h exposure plus washing and additional 24-h incubation. Lysosomes were stained by using LysoTracker Green, which is a green-fluorescent dye for labeling and tracking acidic organelles in live cells. The blocking group has 0.1 mM of free folic acid. (F) Drug stability of EC112002 in plasma from mice, rats, dogs, monkeys, and humans was measured for 48 h at 37 °C under shaking. (G) Cathepsin-B-based cleaving rate of EC112002 with $t_{1/2}$ estimated to be 1.4 h. (H) Long-term storage stability of EC112002 in normal saline (0.9% NaCl), measured by RP-HPLC. (I) Representative *in vivo* PET/CT images over 72 h of ^{89}Zr-labeled EC112002 in healthy nude mice (n = 3). White arrowheads point to the heart, bladder, and liver. (J) Biodistribution of ^{89}Zr-DFO-EC112002 in healthy nude mice at 2 and 24 h postinjection (n = 3).

ADCs, which include limited drug-to-antibody ratios (DAR), drug-linker instability, unfavorable pharmacokinetics,[6] and, most critically, the heterogeneous distribution of ADCs in tumor tissues.[7] To date, development of polymeric-based nanodrug delivery systems (DDS), e.g., including BIND-014[8,9] and CRLX101,[10,11] as well as tumor-targeted liposomal drugs, e.g., MM-302,[12,13] have been unsuccessful and were either being terminated after phase I clinical trials or were associated with limited efficacy in phase II clinical trials. Recent advances in the understanding of tumor biological barriers and

https://doi.org/10.1021/acsnano.2c05342
ACS Nano XXXX, XXX, XXX−XXX

evaluation of the varied performance of approved or investigational new drugs (IND)[14,15] have led to the general acceptance that enhancing solid tumor penetration will be a critical aspect for the successful design of next-generation DDS.[16] Although delivery platforms in the ultrasmall (<10 nm) size range have long been considered to have the potential to enhance diffusion and penetration into tumors,[17] major challenges, e.g., in the design, candidate(s) screening/identification, chemistry, manufacturing and controls (CMC), analytical technology, large-scale synthesis and quality control, and IND-enabling toxicology, have hindered their development and clinical translation.

Folate receptor alpha (FRα), a member of the folate receptor family, is a 38−40 kDa glycosyl-phosphatidylinositol (GPI)-anchored cell-surface glycoprotein[18] encoded by FOLR1. It has a restricted distribution in healthy tissues but is overexpressed in a number of solid tumors, including ovarian, endometrial, breast, and lung cancers. This makes FRα an attractive target for anticancer drug development.[19,20] To date, there have been several early- and late-phase clinical trials involving FRα-targeted therapies using ADCs and small-molecule-drug conjugates, including STRO-002 (phase I completed), Vintafolide (EC145, terminated in phase III, PROCEED trial),[21,22] and mirvetuximab soravtansine (IMGN853). Among these, ImmunoGen's mirvetuximab soravtansine is the most advanced with a completed single agent phase II registrational enabling trial (SORAYA). The positive top line data were announced in 2021 with favorable safety and efficacy in the treatment of patients with folate receptor alpha (FRα)-high platinum-resistant ovarian cancer who have been previously treated with Avastin (bevacizumab).[23−26]

In the current study, we describe the development and *in vitro*/*in vivo* characterization of an ultrasmall folate receptor targeted nanoparticle drug conjugate, referred to as folic acid (FA) functionalized C'Dot-drug-conjugates, or folic acid CDC.

RESULTS AND DISCUSSION

Design of Ultrasmall FRα-Targeted CDC. In its final form, folic acid CDC is approximately 6 nm in diameter and is comprised of three critical components, as shown in Figure 1A and Figure S1A:

- **Ultrasmall clickable silica carrier**: A C'Dot carrier is an ultrasmall poly(ethylene glycol) surface-functionalized (PEGylated) silica nanoparticle encapsulating one to two (~1.8 molecules on average) Cy5 fluorescent dyes that are covalently bound to the silica network.[27,28] The Cy5 dye facilitates the ultrasmall particle synthesis and characterization and enables optical detection of the CDC in preclinical studies and clinical trials. The PEG-based organic shell has been further functionalized with dibenzocyclooctyne (DBCO) groups to endow the silica carrier with a clickable surface.
- **Multiple noncleavable targeting moieties**: The FR-targeting moiety is a folic acid molecule functionalized with a noncleavable PEG spacer and an azide terminal group, which is capable of reacting with the DBCO group on the C'Dot carrier surface to form a covalent bond (Figure 1A). Folic acid CDC was designed to conjugate multiple FR-targeting moieties to enhance its active targeting via multivalency effects.
- **Multiple cleavable exatecan drug linkers**: Exatecan is the cytotoxic agent (pharmacologic class: topoisomerase 1 inhibitor) warhead of the molecularly engineered drug linker, which is composed of a proteolytically cleavable dipeptide linker and a clickable azide group. The exatecan drug linker is designed to be labile in the presence of the enzyme cathepsin B (Cat-B), which is overexpressed in the lysosome of many cancers. Cat-B hydrolyzes the dipeptide linker to release the free cytotoxic exatecan payload. Folic acid CDC was molecularly engineered to conjugate a higher concentration of payloads than the ADC that have been approved to date, i.e., Enhertu (trastuzumab deruxtecan, DAR = 8).[29]

Lead Candidate EC112002 Characterizations. Over 70 variants of drug linkers with two different topoisomerase-1 inhibitor warheads, linker types, and cleavage mechanisms and more than 500 folic acid CDC formulations were developed and evaluated *in vitro*. From these studies, a lead folic acid CDC candidate with promising potency, stability, and specificity properties was identified and was designated EC112002. On average, EC112002 was composed of 13 folic acid and 21 cathepsin-B enzyme cleavable exatecan drug linkers, respectively. The average particle size of EC112002 as determined by fluorescence correlation spectroscopy (FCS) was 6.4 nm (Figure S1B).[30,31] UV−vis absorbance spectra of EC112002 exhibited two characteristic absorption peaks at wavelengths around 647 and 360 nm, corresponding to Cy5 dye and the exatecan payload, respectively (Figure S1C). For the analysis of EC112002 purity and the nature of impurities, reverse phase HPLC (RP-HPLC) coupled to a photodiode array detector was used.[32] A representative chromatogram of EC112002 with a purity >99.0% is shown in Figure S1D. Figure 1B shows a representative transmission electron microscopy (TEM) image of EC112002, where each dark dot represents a single EC112002 nanoparticle−drug conjugate. The inset in Figure 1B depicts a photo of EC112002 in the selected container−enclosure system, exhibiting a characteristic blue color from encapsulated Cy5 dye.

Next, we studied FRα specific binding, multivalency effects, enzymatic payload cleavage, plasma stability, *in vivo* clearance, and biodistribution of EC112002. The flow cytometry results in Figure 1C showed highly specific FRα binding of EC112002 (1 nM) to KB cells (human cervical adenocarcinoma overexpressing FRα) after a 60 min incubation at 4 °C, while the nontargeted control particles with the same amount of payload but no FA ligands showed minimal binding under the same conditions. The specificity of EC112002 for cell surface FRα was confirmed by the addition of 1 mM free FA, which blocked EC112002 binding (Figure 1C). Varying the folic acid CDC drug-to-particle ratios (DPRs) from <10 to close to 40 showed little impact on the targeting of FRα (Figure S2A). When more than 10 FA molecules were conjugated to folic acid CDC, a multivalency effect was observed, resulting in an over 40-fold enhancement of FRα binding strength as compared to free FA (Figure 1D). Increasing the average FA ligand number from 12 to 25 did not significantly increase the binding strength of the folic acid CDC (Figure S2B). Specific FRα binding and intracellular lysosomal trafficking were demonstrated by using confocal microscopy. After a 1 h exposure of KB (FRα positive) or TOV-112D (FRα negative) cells with EC112002, specific binding of EC112002 to the surface of FRα positive KB cells, but not to the FRα negative TOV-112D cells, was observed (Figure 1E, top panel). Internalization and lysosomal trafficking of EC112002 in the KB cells were confirmed by the reduction of the cell surface membrane signal of EC112002 and colocalization of EC112002 (red color in the image) with a commercial agent that localizes in the lysosome of living cells

https://doi.org/10.1021/acsnano.2c05342
ACS Nano XXXX, XXX, XXX−XXX

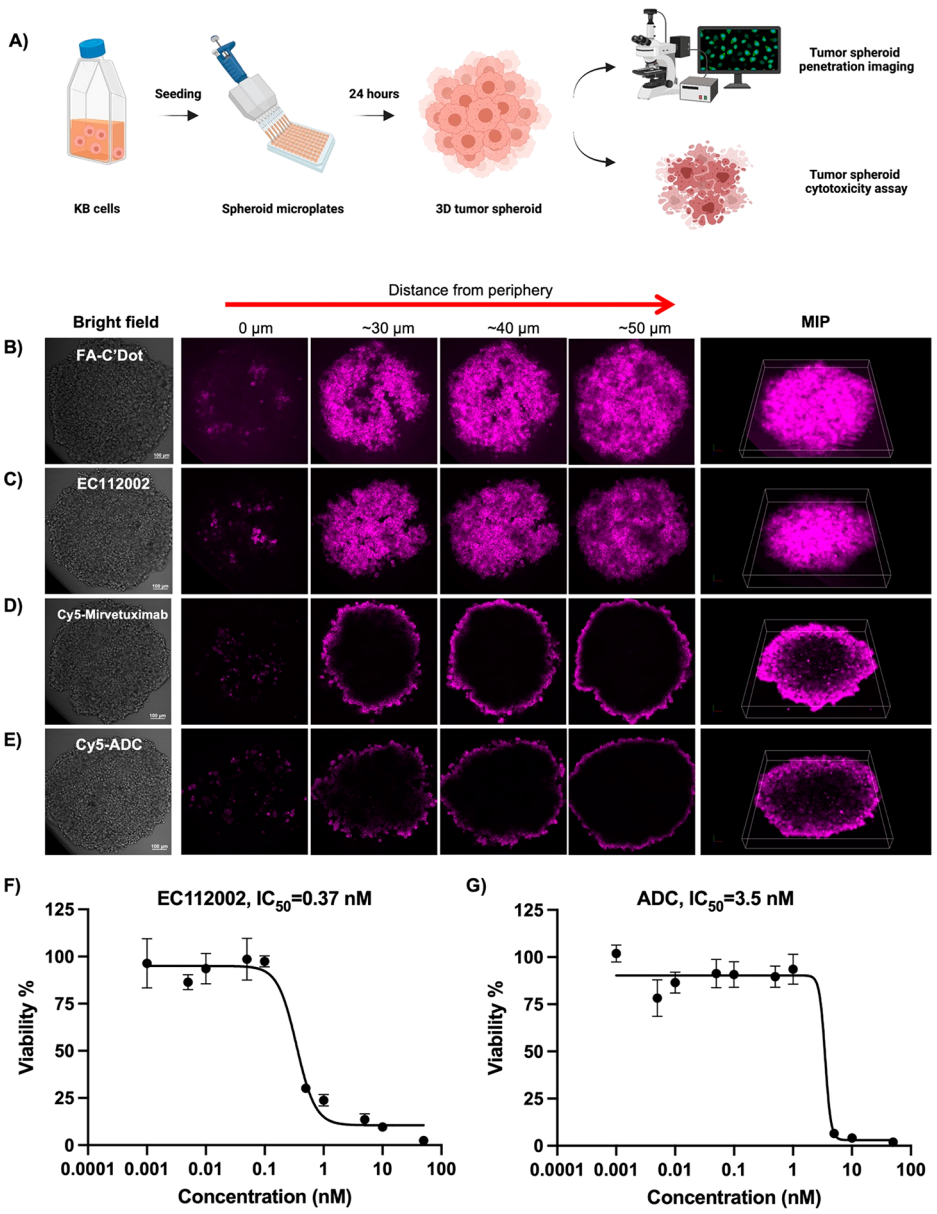

Figure 2. Comparison of ex vivo KB tumor spheroid penetration/therapeutic efficacy between EC112002 and anti-FRα ADC. (A) Schematic illustration of 3D tumor spheroid generation and penetration/efficacy study (created with BioRender.com). Z-stacks of confocal microscopy images of a KB tumor spheroid treated with (B) FA-C'Dot, (C) EC112002, (D) Cy5-mirvetuximab, and (E) Cy5-mirvetuximab-DM4 (Cy5-ADC) at 37 °C for 4 h (concentration: 50 nM), followed by washing; scale bar: 100 μm. Both Cy5-mirvetuximab and Cy5-ADC were prepared by reacting Cy5-NHS ester with either mirvetuximab or ADC and subsequent purification using a PD-10 column. MIP: maximum intensity projection. (F and G) 3D KB tumor spheroid cytotoxicity comparison between EC112002 and ADC.

(LysoTracker, green color in the image; Figure 1E, bottom panel). No obvious membrane binding of EC112002, nor internalization/lysosomal trafficking, was observed in the FRα negative TOV-112D cells or in the FRα positive KB cells that were blocked with 0.1 mM of free FA. Taken together, our results demonstrate highly specific FRα active targeting, multivalency effects, internalization, and lysosomal trafficking of EC112002 in FRα positive cancer cells.

As with ADCs, a balance between the cleaving rate/payload release in the presence of the Cat-B and linker stability in storage and in human plasma is critical to the performance of CDCs. As shown in Figure 1F, the plasma stability of EC112002 was evaluated in a panel of species. EC112002 was observed to be very stable in plasma with the greatest stability observed in human plasma with nearly zero percent exatecan released over a 48-h incubation *in vitro* with shaking at 37 °C. The stability in other species in decreasing order was monkey > rat > dog > mouse with ~10% cleaved exatecan observed in mouse plasma after 48 h. The latter effect is the result of the presence of specific enzymes in mouse plasma, which hydrolyze the dipeptide linker of EC112002. The half time, $t_{1/2}$, of the cleaving rate of EC112002 in the presence of a significant excess of activated cathepsin-B enzyme was estimated to be 1.4 h (Figure 1G). Additionally, EC112002 was observed to be stable for over 6 months when stored in sterile saline solution at 4 °C (Figure 1H). To verify that EC112002 maintained the biodistribution and renal clearance profiles previously reported for C'Dots, we conjugated chelator

https://doi.org/10.1021/acsnano.2c05342
ACS Nano XXXX, XXX, XXX−XXX

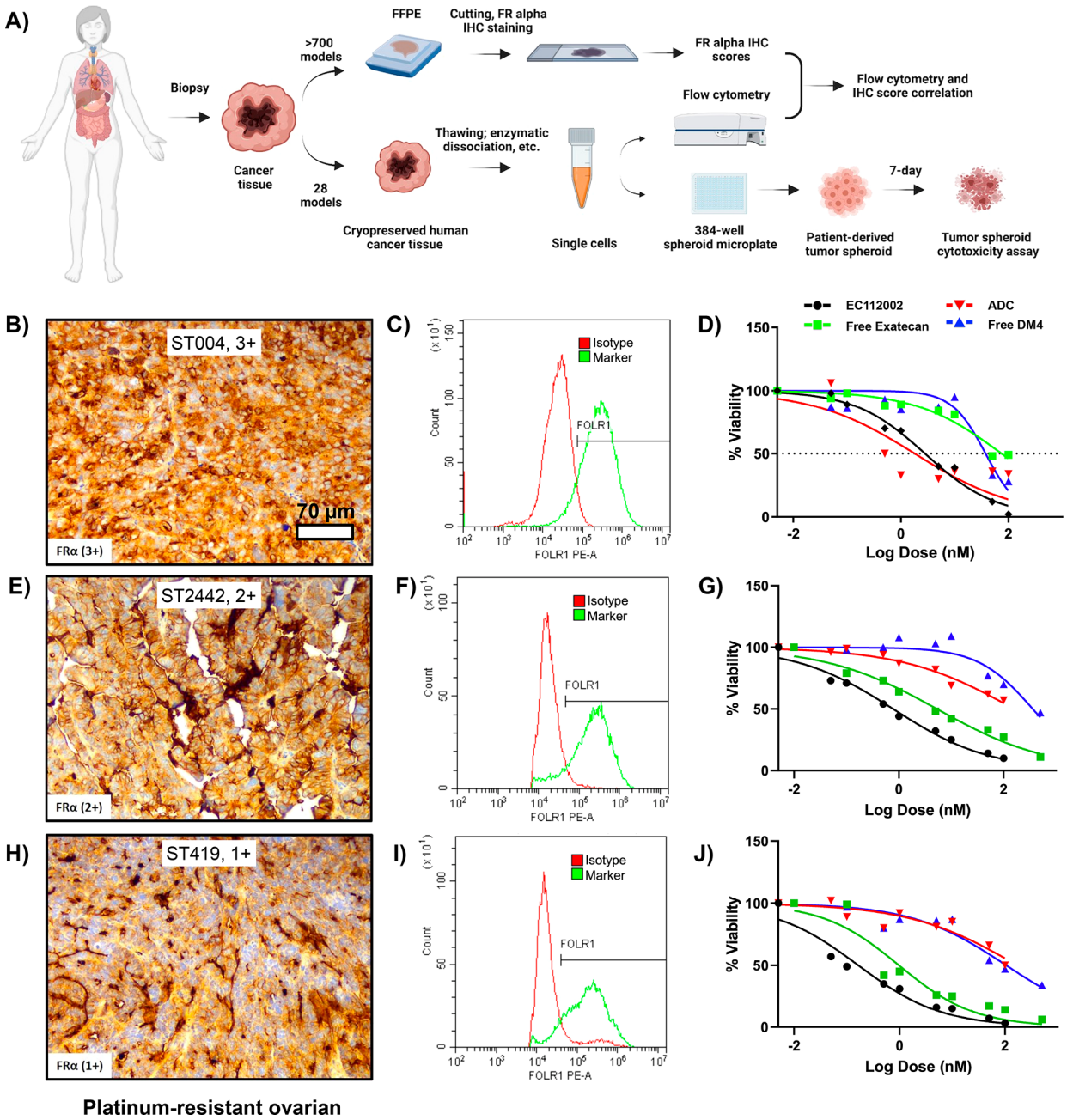

Figure 3. ***Ex vivo*** **efficacy comparison between EC112002 and ADC in patient-derived tumor spheroids of platinum-resistant ovarian, endometrial, non-small-cell lung, breast and triple-negative breast, and head and neck cancers. (A) A schematic illustration of the study workflow (created with BioRender.com). (B, E, and H) ICH images of FFPE slides from platinum-resistant ovarian with varied FR*α* expression levels. (C, F, and I) Flow cytometry histograms of cell suspension digested from the corresponding cancer models. (D, G, and J) 3D tumor spheroid cytotoxicity curves of corresponding cancer models treated with EC112002, free exatecan, anti-FR*α* ADC, and free DM4.**

deferoxamine (DFO) to EC112002 and labeled it with a zirconium-89 (^{89}Zr, $t_{1/2}$ = 78.4 h) radioisotope for *in vivo* PET imaging and biodistribution studies using previously published protocols.[33−37] The whole-body PET/CT images presented in Figure 1I revealed activity in the mouse heart and urinary bladder activity at 1 h postinjection (p.i.), indicating the presence of EC112002 in the circulatory system and clearance through the kidneys into the urine. As is consistent with a rapid renal elimination and a lack of normal tissue distribution and retention, a significant reduction was observed in radioactive signal in the PET images between the 1-h p.i. and 24-h p.i. time points. The quantitative biodistribution profiles of EC112002 in healthy mice at 2 and 24-h p.i. time points, as determined by necropsy, dissection, and radioactive counting, are compared in Figure 1J, and results are summarized in Table S2. This study showed that EC112002 was not significantly retained in any critical organ.

Enhanced Penetration in 3D Cell-Line-Derived Tumor Spheroids. The *in vitro* potency of EC112002 was evaluated against a panel of commercially available cell lines spanning a range of FR*α* expression. In these studies, an anti-FR*α*-DM4 ADC was employed as a comparator. The comparator ADC was developed and produced for these studies by Syngene International Ltd. based upon the published patent profile of

https://doi.org/10.1021/acsnano.2c05342
ACS Nano XXXX, XXX, XXX−XXX

Table 1. Summary of *Ex Vivo* Tumor Spheroid Treatment Efficacy[a]

cancer type	model	FR alpha positivity (IHC score)	cytotoxicity IC_{50} (nM)				differences in potency		differences in potency	
			EC112002	ADC	exatecan	DM4	exatecan vs. EC112002	mean	DM4 vs. ADC	mean
ovarian	ST004	3+	2.8	1.8	74.7	37.6	26.6		20.8	
ovarian	ST3308	3+	1.8	NR	7.7	76.1	4.4			
ovarian	ST024	3+	0.4	NR	3.9	NR	9.6	13.5		20.8
ovarian	ST182B	2+	0.2	2.4	0.7	9.2	4.4		3.9	
ovarian	ST206	2+	17.4	39.8	202.8	87.4	11.7		2.2	
ovarian	ST2442	2+	0.8	159.6	1.7	94.6	2.2	6.1	0.6	2.2
ovarian	ST182	1+	0.3	3.4	2.8	NR	8.5			
ovarian	ST419	1+	0.16	171.3	0.34	33.1	2.1		0.2	
ovarian	ST4321	1+	0.3	36.4	0.7	43.3	2.4	4.3	1.2	0.7
endometrium	ST1392	3+	0.39	3.42	3.44	34.32	8.8		10.0	
endometrium	ST2043	3+	36.6	NR	409.5	128.9	11.2			
endometrium	ST4413	3+	2.47	5.52	25.82	12.52	10.5	10.2	2.3	6.2
endometrium	ST2073	2+	3.15	58.3	7.9	65.3	2.5		1.1	
endometrium	ST2136	2+	6.13	NR	21.4	NR	3.5			
endometrium	ST2846	2+	0.80	57.70	16.67	188.20	20.8	8.9	3.3	2.2
NSCL	ST1931	3+	0.25	40.75	2.13	51.04	8.5		1.3	
NSCL	ST1989	3+	2.4	40.52	17.4	366.2	7.3	7.9	9.0	5.1
NSCL	ST1243	2+	0.46	6.00	4.74	43.23	10.3		7.2	
NSCL	ST3647	2+	0.31	12.45	2.87	41.67	9.3		3.3	
NSCL	ST3898	2+	4.04	634.40	61.6	NR	15.2	11.6		5.3
breast (HR-, HER2+)	ST353	2+	1.69	NR	5.79	139.00	3.4			
breast (HR+, HER2+)	ST430	2+	0.42	NR	1.58	19.94	3.8			
breast (HR+, HER2+)	STF040	2+	3.18	25.11	33.64	33.98	10.6	5.9	1.4	1.4
TNBC	ST1248	1+	1.93	18.21	161.9	32.7	83.9		1.8	
TNBC	ST1599	1+	3.20	25.56	157.5	29.4	49.2	66.6	1.2	1.5
head and neck	ST1203	2+	0.22	3.55	2.29	24.88	10.4		7.0	
head and neck	ST2216	2+	1.21	153.90	9.74	270.40	8.0		1.8	
head and neck	ST2430	2+	0.37	68.67	2.0	166.9	5.3	7.9	2.4	3.7

[a]NSCL, non-small-cell lung cancer; TNBC, triple-negative breast cancer; NR, no response.

mirvetuximab soravtansine (IMGN853, U.S. patent US9637547B2; ImmunoGen, Inc.).[38] This ADC contains a 4-(pyridin-2-yldisulfanyl)-2-sulfo-butyric acid (sSPDB) linker and the maytansine drug, DM4, at a DAR of ∼4:1. Results presented in Figure S3 revealed that EC112002 exhibited greater potency than the ADC under nearly all cell lines and conditions with the exception of a short exposure in the agents in the KB (high FRα) cell line—possibly due to the differences in receptor binding and internalization rates.

Next, we generated a three-dimensional (3D) human cervical adenocarcinoma KB spheroid model for comparison of the penetration and efficacy of EC112002 and the anti-FRα ADC. It is generally accepted that a 3D spheroid model (1) may more accurately reflect the complex *in vivo* microenvironment of a tumor; (2) may contain proliferative gradients, hypoxia, and necrosis that occur in naturally occurring tumors; and (3) can be used to at least partially reproduce, analyze, and achieve the resolution needed to see penetration/distribution differences of different drugs and DDS.[39] Noting the challenges in controlling the dosing level, difficulties in optimizing the tissue collection time window, the potential loss of fluorescent signal during sample preparation, and the lack of well-accepted mathematical analysis tools for penetration comparison, a direct fluorescent-based penetration comparison between EC112002 and anti-FRα ADC in solid tumor tissue was not employed in our current research. As schematically shown in Figure 2A, we used Corning ultralow attachment surface 96-well spheroid microplates for the generation of KB spheroids at a cell density of ∼10 000 cells/well. Formation of the tumor spheroid was achieved within 24 h of incubation at 37 °C and validated by using optical microscopy.

Figure 2B–E show Z stacks (1 μm/step) of confocal images of each KB spheroid (∼800 μm in diameter) treated with FA-C'Dots (payload-free FRα-targeted C'Dots), EC112002, Cy5-Mirvetuximab, and Cy5-Mirvetuximab-DM4 (also named Cy5-ADC). Clear differences were observed in drug penetration/diffusion patterns when comparing FA-C'Dots with Cy5-Mirvetuximab (both payload-free) and EC112002 with Cy5-ADC (both payload-conjugated). The FA-C'Dots without payload and EC112002 both exhibited uniform penetration and binding to nearly all of the KB cells throughout each spheroid (Videos S1 and S2). In stark contrast, both Cy5-Mirvetuximab and Cy5-ADC only penetrated a few cell layers of the spheroid model, leading to a ring-shaped fluorescence distribution pattern around the rim of the spheroid with a large nonfluorescent center of the spheroid (Videos S3 and S4). Considering that both EC112002 and Cy5-ADC target cell surface FRα with a comparable binding strength, the neutral surface charge of the C'Dots and, possibly more importantly,

https://doi.org/10.1021/acsnano.2c05342
ACS Nano XXXX, XXX, XXX−XXX

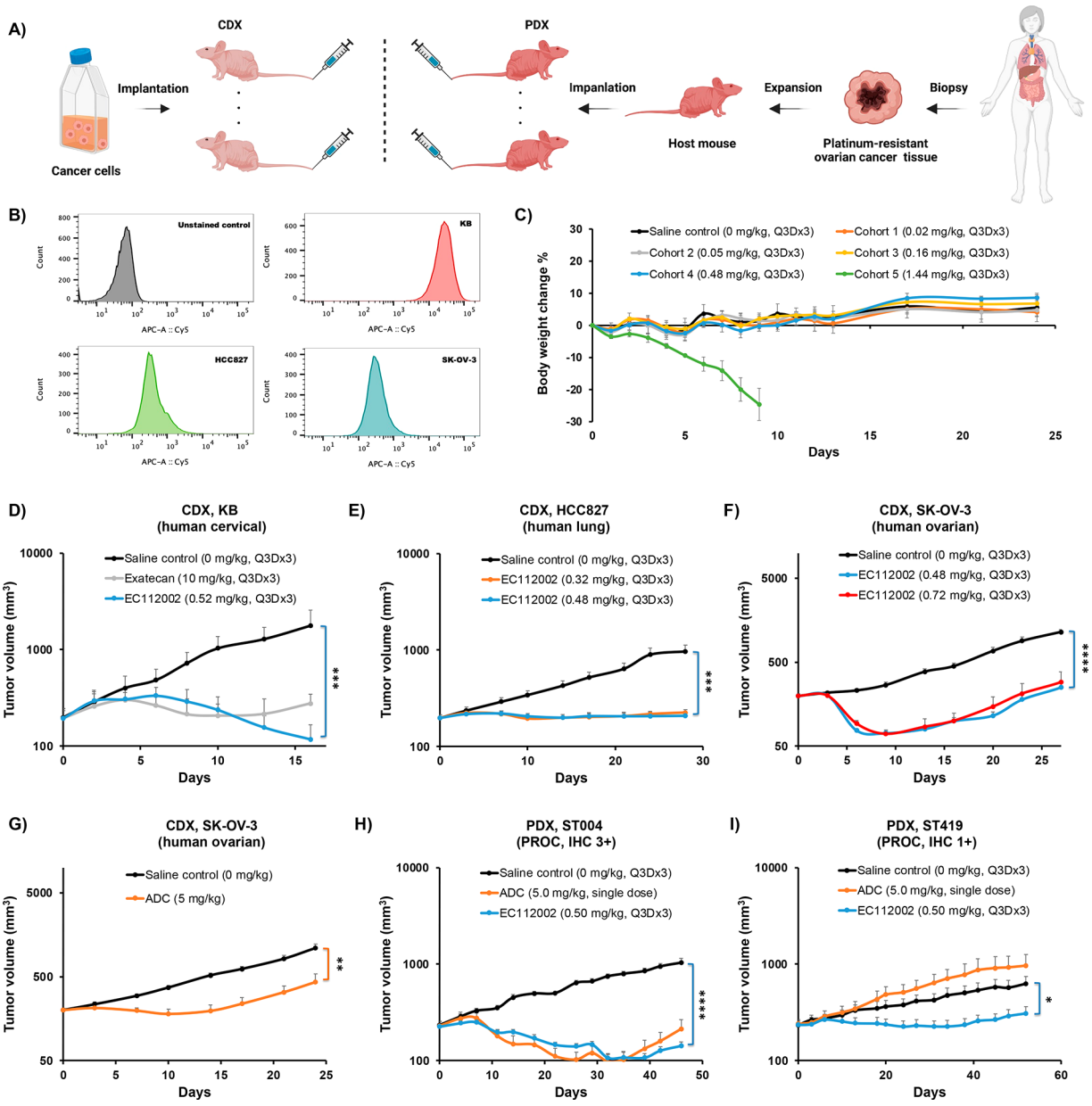

Figure 4. ***In vivo*** **efficacy comparison between EC112002 and ADC in cell-line- and patient-derived xenograft tumor models. (A) A schematic illustration of the generation of cell-line-derived and patient-derived xenograft small animal models (created with BioRender.com). (B) Flow cytometry of EC112002 in human lung (HCC827), ovarian (SK-OV-3), and cervical (KB) cancer cell lines against unstained cell control. Flow cytometry conditions were 100 nM, 4 °C, and 60 min incubation. KB cell line showed expected high FR*α* expression, while both HCC827 and SK-OV-3 showed medium to low FR*α* expression levels. (C)** ***In vivo*** **maximum tolerated dose study of EC112002 in healthy nude mice. The dose (mg/kg) was based on conjugated exatecan. (D)** ***In vivo*** **efficacy comparison between free exatecan at about 20-fold higher dose level (i.e., 10 mg/kg, Q3Dx3) and EC112002 (0.52 mg/kg, Q3Dx3) in KB tumor-bearing mice. (E)** ***In vivo*** **efficacy of EC112002 at MTD (0.48 mg/kg, Q3Dx3) and 2/3 of MTD (0.32 mg/kg, Q3Dx3) in HCC827 human lung cancer bearing mice. (F)** ***In vivo*** **efficacy of EC112002 at MTD (0.48 mg/kg, Q3Dx3) and 1.5-fold of MTD (0.72 mg/kg, Q3Dx3) in SK-OV-3 human ovarian cancer bearing mice. (G)** ***In vivo*** **efficacy of anti-FR*α* ADC (5.0 mg/kg, single dose) in SK-OV-3 human ovarian cancer bearing mice. (H)** ***In vivo*** **efficacy comparison between anti-FR*α* ADC (5.0 mg/kg, single dose) and EC112002 (0.50 mg/kg, Q3Dx3) in a platinum-resistant ovarian cancer PDX model (ST004) with an IHC score of 3+. (I)** ***In vivo*** **efficacy comparison between anti-FR*α* ADC (5.0 mg/kg, single dose) and EC112002 (0.50 mg/kg, Q3Dx3) in a platinum-resistant ovarian cancer PDX model (ST419) with an IHC score of 1+.**

their ultrasmall particle size may play key roles in achieving the observed greater penetration depth in the 3D tumor spheroid models. Consistent with the observation of greater tumor penetration, the cytotoxicity of EC112002 was observed to be approximately 10-fold greater than that of the ADC in the KB cell tumor spheroid model (Figure 2F,G).

Enhanced Efficacy in 3D Patient-Derived Tumor Spheroids. *In vivo* patient-derived xenograft (PDX) small animal models are histologically and genetically closer to a patient's original tumor[40,41] and to tumors encountered in clinical trials than cell-line-derived xenograft (CDX) models. As such, these models may provide a more predictive assessment of future clinical drug responses. However, as

https://doi.org/10.1021/acsnano.2c05342
ACS Nano XXXX, XXX, XXX−XXX

compared to CDX models, *in vivo* PDX models are associated with a number of significant challenges including their often extremely slow growth rates, lower rates of successful implantation in the animals, and comparatively significantly high costs. *Ex vivo* 3D patient-derived tumor spheroids can provide an alternative to 2D-cultured cell line models that achieve many of the benefits of *in vivo* PDX models including the ability to better simulate a more natural *in vivo* tumor microenvironment that can have an impact on the potency of a study drug while simultaneously maintaining a rapid ∼1 week assay.[42] As shown in Figure 3A, formalin-fixed paraffin-embedded (FFPE) tumor tissue slides from >700 patients of nine different cancer indications that are known to potentially overexpress FRα were selected for immunohistochemistry (IHC) staining and scoring following published procedures.[43] A total of 28 PDX models from different indications (i.e., platinum-resistant ovarian, endometrial, non-small-cell lung, breast, triple-negative breast, and head and neck cancers) were selected based on drug-resistant profiles and FRα positivity and were employed in a KIYA-PREDICT (Kiaytec Inc., Greenville, SC) 3D tumor spheroid cytotoxicity assay.[42]

Platinum-resistant ovarian cancer (PROC) was selected as the primary cancer indication in the current study. FRα is overexpressed in 70−80% of epithelial ovarian cancers, and expression has been shown to significantly correlate with histological grade and stage.[44] Women with PROC continue to have a poor prognosis, and effective and tolerated treatments for PROC remain a substantial unmet need.[45] As shown in Figure 3 and Figure S4, a total of nine PROC models with IHC scores of 1+ (n = 3), 2+ (n = 3), and 3+ (n = 3) were selected for 3D tumor spheroid model generation and cytotoxicity assays between EC112002 and anti-FRα ADC. Cytotoxicity studies of free exatecan (EC112002 warhead) and free DM4 (ADC warhead) were also performed in the same models, to compare the intrinsic sensitivity of the models to the warheads. Although a high correlation between the IHC scoring and the FRα flow cytometry is not always possible when the two methods were performed by two different contract research organizations using different anti-FRα antibodies and different quantification methods, the results of these studies generally correlated as the models with higher IHC scores showed higher delta median fluorescent intensity (MFI), indicating that the enzymatically digested cell mixtures contained cells with higher FRα expressions (Figures 3, S4, and S5A).

As detailed in Figure 3, Figure S4, and Table 1, 3D patient-derived tumor spheroid cytotoxicity assays revealed an association between the IHC scores and cytotoxicity resulting from either EC112002 or ADC treatment. In these studies, higher IHC scores (i.e., higher FRα expression) were generally associated with higher cytotoxic efficacy. Among the nine tested PROC models, the IC_{50} of EC112002 ranged from 160 pM (Model ID: ST419) to 17.6 nM (Model ID: ST206). The high potency of anti-FRα ADC was also observed with a single-digit IC_{50} value in the 3+ model (ST004). Interestingly, anti-FRα ADC showed no response in two (ST3308 and ST204) of the three 3+ PROC models (possibility due to the heterogeneity of patient-derived cancer tissue and the reduced sensitivity of the DM4 warhead in certain models), for which EC112002 was demonstrated to still be potent with IC_{50} values of 1.8 and 0.4 nM, respectively. According to a recent phase III clinical trial of anti-FRα mirvetuximab soravtansine ADC,[26] a lower level of efficacy was observed in patients with a medium to low FRα expression in their tumors. This was also confirmed in our study, where the target/free ratio of EC112002 was found to be 6-fold higher than the same ratio from anti-FRα ADC in the 1+ models. In these studies, EC112002 revealed the ability to potently kill patient-derived cancer cells with low FRα IHC scores potentially overcoming cancer heterogeneity via enhanced penetration into, and diffusion across, solid tumors.

The cytotoxicity of EC112002 and the anti-FRα ADC were evaluated in patient-derived 3D tumor spheroids from other cancer indications reported to potentially overexpress FRα including endometrial, non-small-cell lung, breast, triple-negative breast, and head and neck cancers. As shown in Figure S4, Table 1, and Figure S5B, a consistently higher potency for EC112002 was observed across indications and FRα IHC scores as compared to the anti-FRα ADC (greater potency in 26 out of 28 selected models). Surprisingly, EC112002 was found to be highly potent in triple-negative breast cancer (TNBC, 1+, ST1248, and ST1599) with a > 50-fold increase in potency for the CDC delivered warhead than for the free warhead, while in the same models no significant difference was observed between the anti-FRα ADC and free DM4. Taken together, the studies presented above demonstrate the enhanced specific cytotoxicity capability of EC112002 as compared with an anti-FRα ADC in 3D patient-derived tumor spheroids.

Enhanced Efficacy in Cell-Line-Derived and Patient-Derived Xenograft Models. We developed EC112002 for the treatment of patients who have advanced, recurrent, or refractory solid tumors that overexpress FRα and are sensitive to topoisomerase 1 inhibition. The expected mechanism of action (MOA) in preclinical small animal models and the ongoing clinical trial involves (1) enhanced tumor penetration due to the permeation and retention effects of EC112002, (2) preferential targeted delivery of the drug to the tumor cells via binding to overexpressed FRα, and (3) effective tumor cell killing via the enzymatically cleaved/released exatecan. We hypothesize that the targeted delivery of EC112002 also affords a mechanism to reduce off-target toxicities in cancer patients by limiting the exposure of normal tissues to the cytotoxic exatecan warhead due to the relatively rapid elimination of EC112002 by the kidneys.

To demonstrate the therapeutic efficacy of EC112002, three CDX models and two PDX models were generated, as illustrated in Figure 4A. The levels of FRα expression in the three CDX models were determined by flow cytometry, where human cervical KB cells showed high FRα expression, and human lung HCC827 and human ovarian SK-OV-3 cells showed medium to low FRα expression (Figure 4B). In the case of the PDX models, ST004 (IHC 3+) and ST419 (IHC 1+) were selected for *in vivo* efficacy studies based on the *ex vivo* PDX tumor spheroids results (shown in Figure 3). Figure 4C summarizes the *in vivo* maximum tolerated dose (MTD) study of EC112002 in heathy nude mice at a dose regimen of Q3Dx3 (one dose every three days, total of three doses). The results showed dose-dependent toxicity with less than 1% of bodyweight loss in mice treated with doses of EC112002 containing up to 0.48 mg of conjugated exatecan/kg of animal body weight, while >20% bodyweight losses were observed in mice treated with EC112002 containing 1.44 mg of conjugated exatecan/kg of body weight on day 9. The MTD was estimated to be between 0.48 mg/kg and 1.44 mg/kg of exatecan conjugated to EC112002.

https://doi.org/10.1021/acsnano.2c05342
ACS Nano XXXX, XXX, XXX−XXX

Table 2. Summary of *in Vivo* EC112002 Treatment Efficacy in CDX and PDX Models

model		drug	dose regimen[a]	dose (mg/kg)[b]	mean % tumor growth inhibition on the day control group tumor volume was close to or >1000 mm^3[c]	safety level
CDX	KB	saline control	Q3Dx3	0		safe
		exatecan	Q3Dx3	10	84.4% on day 16	toxic
		EC112002	Q3Dx3	0.52	93.4% on day 16	MTD
	HCC827	saline control	Q3Dx3	0		safe
		EC112002	Q3Dx3	0.32	76.8% on day 28	2/3 MTD
		EC112002	Q3Dx3	0.48	78.5% on day 28	MTD
	SK-OV-3	saline control	Q3Dx3	0		safe
		EC112002	Q3Dx3	0.48	78.1% on Day 27	MTD
		EC112002	Q3Dx3	0.72	74.7% on day 27	toxic
	SK-OV-3	saline control	Q3Dx3	0		safe
		ADC	single dose	5.0	60.6% on day 24	MTD
PDX	ST004, 3+	saline control	Q3Dx3	0		safe
		EC112002	Q3Dx3	0.5	86.2% on day 46	MTD
		ADC	Q3Dx3	5.0	79.4% on day 46	MTD
	ST419, 1+	saline control	Q3Dx3	0		safe
		EC112002	Q3Dx3	0.5	50.7% on day 52	MTD
		ADC	Q3Dx3	5.0		MTD

[a]Q3Dx3 = 3 total doses with each dose given every 3 days. [b]Dose based on amount of conjugated exatecan in nanoparticle. [c]Mean % Inhibition = $(\text{mean}(C) - \text{mean}(T))/\text{mean}(C) \times 100\%$. T, current group value. C, control group value.

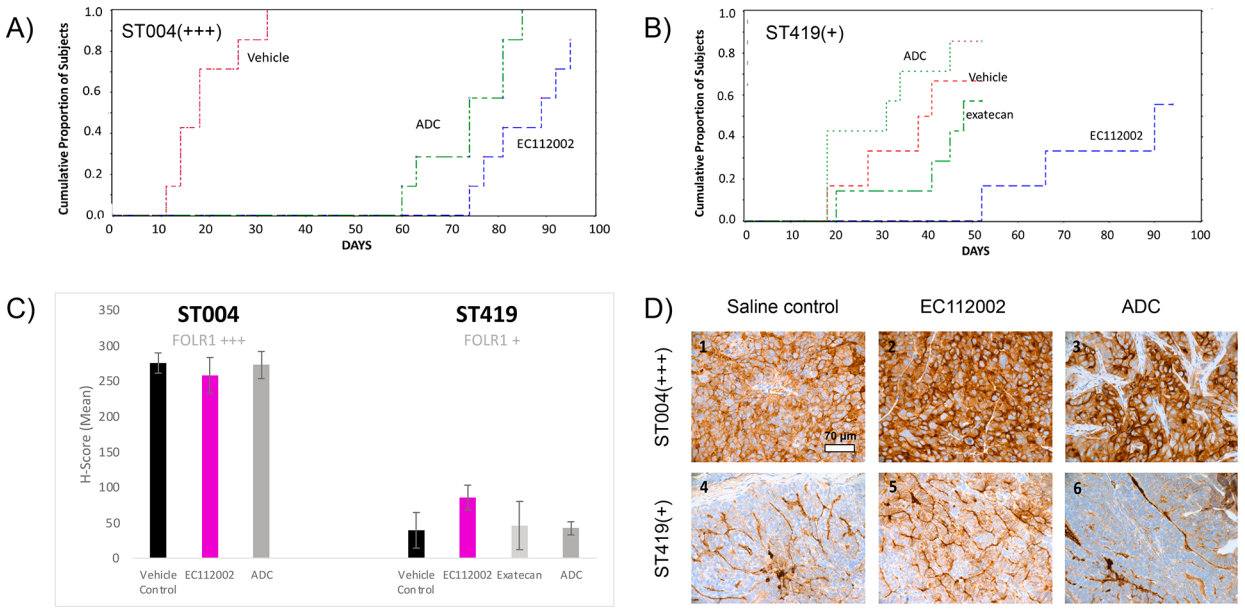

Figure 5. Kaplan–Meier survival analysis of the EC112002 in two PDX models and related folate receptor alpha IHC staining. Kaplan–Meier estimates of time to 2× baseline tumor volume or death in PDX models of (A) ST004 and (B) ST419. (C) The H-score of tumors from mice after the single-cycle treatment. (D) IHC staining images of tumors from ST004(3+) and ST419(1+) PDX models with different kinds of treatments.

To demonstrate that the C'Dot drug delivery platform can improve the therapeutic efficacy of a warhead while reducing its toxicity as compared to the warhead administered as a free drug, we compared the *in vivo* safety and tumor growth inhibition of EC112002 and free exatecan. Mice bearing subcutaneous human cervical KB (FRα high) CDX tumors were generated and treated by intravenous (i.v.) bolus administration with free exatecan at 10 mg/kg (Q3Dx3) or EC112002 at nearly 1/20th of the dose of exatecan, i.e., 0.52 mg/kg (Q3Dx3). Figure S6A summarizes the bodyweight changes over the study period, where the free exatecan cohort exhibited significant bodyweight losses, indicating the high off-target side effects of free exatecan. In contrast, only minor (~5%) bodyweight loss was observed following the administration of EC112002 (Figure S6A). As depicted in Figure 4D, mice treated with both free exatecan (at a dose considered to

https://doi.org/10.1021/acsnano.2c05342
ACS Nano XXXX, XXX, XXX–XXX

be toxic) and EC112002 (at approximately the MTD) showed significant tumor growth inhibition (Figure S7A) with 84.4 and 93.4 mean % tumor growth inhibition on day 16, respectively (Table 2), while tumor volume in the saline control group reached >1000 mm^3 on the same day. Taken together, the studies described above demonstrated that EC112002 was associated with therapeutic efficacy and significantly improved tolerability as compared with a ~20× greater dose of free warhead.

The *in vivo* efficacy of EC112002 was then assessed in mice bearing tumors with medium to low FRα expression levels. As summarized in Figure 4E and F, EC112002 mediated potent tumor growth inhibition (78.5% and 78.1%) on day 28 in HCC827 (lung) and on day 27 in SK-OV-3 (ovarian) at an MTD dose of 0.48 mg/kg, administered by i.v. bolus on a Q3Dx3 schedule (Figure S7B,C). Interestingly, similar efficacy was observed when mice were treated at 2/3 of MTD (in the case of HCC827, Figure 4E), suggesting a potentially broad therapeutic window. Mice treated at 3/2 of MTD (in the case of SK-OV-3) showed >10% bodyweight loss (Figure S6C) but no significant additional therapeutic benefit (78.1% vs 74.7% around day 27; Figure 4F and Table 2). Consistent with the *in vitro* results presented above, EC112002 showed greater therapeutic efficacy as compared to the anti-FRα ADC in SK-OV-3 model tumor-bearing mice with medium to low FRα expression levels, with a significant reduction in tumor volume in the mice treated with EC112002 compared with a minimal reduction of volume and tumor growth delay with the anti-FRα ADC (Figure 4G). By the conclusion of the study, the % mean tumor growth inhibition was estimated to be 78.1% and 60.6%, respectively, for EC112002 and the anti-FRα ADC (Table 2).

Similar therapeutic advantages of EC112002 over ADC were observed in more clinically relevant PDX models. As shown in Figure 4H,I and Figure S7E,F, EC112002 administered by i.v. bolus injection (0.5 mg/kg based upon exatecan concentration, Q3Dx3) was able to achieve slightly higher % mean tumor growth inhibition than the ADC administered by i.v. bolus injection (5 mg/kg; 86.2% vs 79.4%, Table 2) in the ST004 PDX model with a FRα IHC score of 3+ even though the ADC was slightly better than EC112002 in the same model in the *in vitro* spheroid study (described above). The median times the 2× baseline tumor volume or death for the vehicle, EC112002, and ADC were estimated to be 18, 89, and 74 days, respectively (Figure 5A). The pairwise comparison of the vehicle vs EC112002 yielded a statistically significant difference of $P = 0.0001$ (Table S3). In the ST419 PDX model with a FRα IHC score of 1+, our results suggested no clear therapeutic response following treatment with the anti-FRα ADC with very similar median tumor volumes observed for both the ADC and saline control groups (Figure S6G). In contrast, EC112002 treatment (0.5 mg/kg based upon exatecan concentration Q3Dx3) resulted in a significant tumor growth delay in the 1+ FRα ST419 model with a % mean tumor growth inhibition estimated to be 50.7% on day 52 (Table 2). The median times the 2× baseline tumor volume or death for the vehicle, EC112002, exatecan, and ADC were 39.5, 90, 48, and 31 days, respectively (Figure 5B). The pairwise comparison of EC112002 vs ADC yielded a statistically significant difference of $P = 0.0153$ (Table S4). The impact of treatment on FRα expression was determined by performing IHC on tumor samples collected at the conclusion of the *in vivo* PDX efficacy studies. As shown in Figure 5C, post-treatment FRα expression in vehicle controls was consistent with prestudy expectations, i.e., ST004 exhibited high FRα 3+ expression and ST419 exhibited low FRα 1+ expression. Post-treatment FRα expression was consistent between the vehicle control and treatment groups, suggesting that EC112002 and ADC treatment did not result in a reduction in FRα levels. This suggests that additional cycles of treatment would have been successful. The results above demonstrate that EC112002 is effective in both the setting of high (3+) FRα expression (model ST004) and low (+1) FRα expression (model ST419), while the FRα ADC was effective only in the PDX model with high FRα expression. Taken together, our *in vivo* efficacy studies demonstrated the superiority of EC112002 over the anti-FRα ADC in both CDX and PDX preclinical animal models. For the *in vitro* and *in vivo* studies described above, we opted to employ an anti-FRα ADC with a DM4 maytansine warhead in order to better compare our potency/efficacy with mirvetuximab soravtansine, which is the furthest advanced anti-FRα ADC in clinical development. A direct comparison of a CDC and an ADC using the same warhead (e.g., both conjugated to exatecan) targeted against the same tumor associated antigen will be considered for future studies.

CONCLUSIONS

In conclusion, an approximately 6-nm-sized ultrasmall folate receptor targeted C'Dot drug conjugate, EC112002, was developed with ~13 folic acid tumor targeting moieties and ~21 exatecan warheads conjugated via a cathepsin-B cleavable linker. EC112002 demonstrated highly specific FRα targeting, multivalent binding to FRα expressing tumor cells, specific enzymatic warhead release, stability in human plasma, and favorable in vivo clearance/normal organ distribution profiles. When compared with an anti-FRα ADC based upon mirvetuximab soravtansine, EC112002 showed significantly better penetration in 3D cell-line-derived tumor spheroids, FRα-dependent cytotoxicity in patient-derived tumor spheroids across multiple cancer indications, and significant therapeutic efficacy in multiple CDX and PDX preclinical animal tumor models. With the growing interest in developing clinically translatable, safe, and efficacious DDSs, EC112002 has the potential to address critical challenges in systemic drug delivery for cancer management.

MATERIALS AND METHODS

Synthesis of Folic Acid CDC. All folic acid CDCs in this research were produced by Elucida Oncology. The detailed synthesis of Cy5-C'Dot is described in our previous publication.[27,28]

Cells and Cell Culture. Human KB (CCL-17), SK-OV-3 (HTB-77), A549 (CCL-185), BT-549 (HTB-122), and TOV-112D (CRL-11731) cell lines were purchased from ATCC (Manassas, Virginia). The IGROV-1 (SCC203) human ovarian carcinoma cell line was purchased from EMD Millipore (Burlington, Massachusetts). Cells were maintained in folic acid free RPMI 1640 media/10% FBS and 1% penicillin/streptomycin, unless otherwise specified.

Cytotoxic Efficacy Study in 3D Patient-Derived Tumor Spheroid. The cytotoxic efficacy comparison among EC112002, free exatecan, ADC, and DM4 was performed by KIYATEC using the KIYA-PREDICT assay. The FRα immunohistochemistry (IHC) scoring of tumor tissue from platinum-resistant ovarian, endometrial, non-small-cell lung, breast, triple-negative breast, and head and neck cancer patients were conducted by XenoSTART by using the Biocare Medical FRα IHC Assay Kit (CAT# BRI4006KAA), following the manufacturer's protocol. A total of 28 PDX models from different indications were selected based on the IHC scores and provided to

https://doi.org/10.1021/acsnano.2c05342
ACS Nano XXXX, XXX, XXX−XXX

KIYATEC for the KIYA-PREDICT assay. Briefly, cryopreserve PDX tumors were thawed and enzymatically dissociated to single cells and plated into 384-well spheroid microplates (Corning). Flow cytometry was also performed to assess the FRα levels among different PDX models. Following the 24 h of spheroid formation, test agents and controls were added at the designed concentration range and incubated for 7 days at 37 °C. After that, the cell viability was measured by CellTiter-Glo 3D (Cat# G9681, Promega, Madison, Wisconsin). The results were analyzed using KIYATEC's proprietary software. IC_{50}'s were determined using nonlinear regression (normalized to untreated control) in GraphPad Prism 9.0.

***In Vivo* Efficacy Studies in Platinum-Resistant Ovarian Cancer Patient-Derived Xenograft Model.** The PDX studies were performed at XenoSTART according to the guidelines approved by the Institutional Animal Care and Use Committee (IACUC) of XenoSTART. The doses and treatment regimens for each group are described in detail in the respective figures. Tumor fragments (approximately 70 mg, ST004 and ST419) were implanted subcutaneously into the flank region of 6−12 weeks old female athymic nude J:NU mice (The Jackson Lab). Mice were stratified into study cohorts when mean tumor volume reached 150−300 mm^3. Saline control and EC112002 (0.5 mg/kg) were administered via intravenous injection on days 0, 3, and 6. Anti-FRα ADC was administered on day 0 at 5 mg/kg (consistent with the preclinical dose/schedule employed for mirvetuximab soravtansine[38]) via intravenous bolus injection. Mice were monitored for overall health status daily, and their tumor volumes were measured twice a week using a digital caliper throughout the experiment.

ASSOCIATED CONTENT

Supporting Information

The Supporting Information is available free of charge at https://pubs.acs.org/doi/10.1021/acsnano.2c05342.

Detailed descriptions of folic acid CDC characterization; RP-HPLC method for plasma stability, saline stability, and forced release testing; plasma stability testing of folic acid CDC; confocal microscopy imaging of EC112002 in cancer cells; *in vitro* flow cytometry cell binding study; *in vitro* CellTiter-Glo cytotoxic assay; ^{89}Zr radiolabeling of DFO-folic acid CDC; *in vivo* static PET/CT and biodistribution studies; 3D tumor spheroid model of KB; *in vitro* 3D tumor spheroid cytotoxic assay; confocal imaging of folic acid CDC in the 3D tumor spheroid model of KB; *in vivo* maximum tolerated dose study; *in vivo* efficacy studies in cell line derived KB; HCC827 and SKOV-3 xenograft models; statistical analysis; supplementary figures and tables (PDF)

Video 1 (MOV)

Video 2 (MOV)

Video 3 (MOV)

Video 4 (MOV)

AUTHOR INFORMATION

Corresponding Authors

Feng Chen − *Elucida Oncology Inc., Monmouth Junction, New Jersey 08852, United States;* orcid.org/0000-0002-0985-9423; Email: fchen@elucidaoncology.com

Kai Ma − *Elucida Oncology Inc., Monmouth Junction, New Jersey 08852, United States*; Email: kma@elucidaoncology.com

Authors

Fei Wu − *Elucida Oncology Inc., Monmouth Junction, New Jersey 08852, United States;* orcid.org/0000-0002-7187-2258

Pei-Ming Chen − *Elucida Oncology Inc., Monmouth Junction, New Jersey 08852, United States*

Thomas C. Gardinier − *Elucida Oncology Inc., Monmouth Junction, New Jersey 08852, United States*

Melik Z. Turker − *Elucida Oncology Inc., Monmouth Junction, New Jersey 08852, United States*

Aranapakam M. Venkatesan − *Elucida Oncology Inc., Monmouth Junction, New Jersey 08852, United States*

Vaibhav Patel − *Elucida Oncology Inc., Monmouth Junction, New Jersey 08852, United States;* orcid.org/0000-0001-9383-1302

Tin Khor − *Elucida Oncology Inc., Monmouth Junction, New Jersey 08852, United States*

Michelle S. Bradbury − *Department of Radiology and Molecular Pharmacology Program, Sloan Kettering Institute for Cancer Research, New York, New York 10065, United States;* orcid.org/0000-0003-3147-4391

Ulrich B. Wiesner − *Materials Science and Engineering, Cornell University, Ithaca, New York 14850, United States; Kavli Institute at Cornell for Nanoscale Science, Cornell University, Ithaca, New York 14853, United States;* orcid.org/0000-0001-6934-3755

Gregory P. Adams − *Elucida Oncology Inc., Monmouth Junction, New Jersey 08852, United States*

Geno Germano − *Elucida Oncology Inc., Monmouth Junction, New Jersey 08852, United States*

Complete contact information is available at: https://pubs.acs.org/10.1021/acsnano.2c05342

Author Contributions

[#]Contributed equally to the work.

Author Contributions

[▽]Contributed equally to the work.

Author Contributions

Conceptualization: F.W., T.G., M.Z.T., A.V., G.P.A., G.G., F.C., K.M. **Methodology:** F.W., P.C., T.G., M.Z.T., A.V., V.P., T.K., G.P.A., G.G., F.C., K.M. **Investigation:** G.P.A., G.G., F.C., K.M. **Visualization:** F.W., P.C., T.G., M.Z.T., A.V., T.K., F.C., K.M. **Supervision:** G.P.A., G.G. F.C., K.M. **Writing-original draft:** F.W., P.C., T.G., M.Z.T., T.K., F.C., K.M. **Writing-review and editing**: all authors.

Notes

The authors declare the following competing financial interest(s): Fei Wu, Pei-Ming Chen, Thomas C. Gardinier, Melik Z. Turker, Aranapakam M. Venkatesan, Vaibhav Patel, Tin Khor, Michelle S. Bradbury, Ulrich B. Wiesner, Gregory P. Adams, Geno Germano, Feng Chen, and Kai Ma hold interest in Elucida Oncology, Inc.

ACKNOWLEDGMENTS

We appreciate the contributions of Frank Lee of a-connect to the study design and interpretation of the results; the support of Paul Rudick, Marion Scocca, and Eliel Bayever at Elucida Oncology; and the fruitful discussions with Prof. Michelle Bradbury at Memorial Sloan Kettering Cancer Center (MSKCC).

REFERENCES

(1) Rosenblum, D.; Joshi, N.; Tao, W.; Karp, J. M.; Peer, D. Progress and challenges towards targeted delivery of cancer therapeutics. *Nat. Commun.* **2018**, *9*, 1410−1422.

(2) Bulbake, U.; Doppalapudi, S.; Kommineni, N.; Khan, W. Liposomal Formulations in Clinical Use: An Updated Review. *Pharmaceutics* **2017**, *9*, 12−72.
(3) Drago, J. Z.; Modi, S.; Chandarlapaty, S. Unlocking the potential of antibody−drug conjugates for cancer therapy. *Nat. Rev. Clin. Oncol.* **2021**, *18*, 327−344.
(4) Torchilin, V. P. Recent advances with liposomes as pharmaceutical carriers. *Nat. Rev. Drug Discovery* **2005**, *4*, 145−160.
(5) Yuan, F.; Leunig, M.; Huang, S. K.; Berk, D. A.; Papahadjopoulos, D.; Jain, R. K. Microvascular permeability and interstitial penetration of sterically stabilized (stealth) liposomes in a human tumor xenograft. *Cancer Res.* **1994**, *54*, 3352−3356.
(6) Beck, A.; Goetsch, L.; Dumontet, C.; Corvaïa, N. Strategies and challenges for the next generation of antibody−drug conjugates. *Nat. Rev. Drug Discovery* **2017**, *16*, 315−337.
(7) Khongorzul, P.; Ling, C. J.; Khan, F. U.; Ihsan, A. U.; Zhang, J. Antibody−Drug Conjugates: A Comprehensive Review. *Mol. Cancer Res.* **2020**, *18*, 3−19.
(8) Autio, K. A.; Dreicer, R.; Anderson, J.; Garcia, J. A.; Alva, A.; Hart, L. L.; Milowsky, M. I.; Posadas, E. M.; Ryan, C. J.; Graf, R. P.; Dittamore, R.; Schreiber, N. A.; Summa, J. M.; Youssoufian, H.; Morris, M. J.; Scher, H. I. Safety and Efficacy of BIND-014, a Docetaxel Nanoparticle Targeting Prostate-Specific Membrane Antigen for Patients With Metastatic Castration-Resistant Prostate Cancer: A Phase 2 Clinical Trial. *JAMA Oncology* **2018**, *4*, 1344−1351.
(9) Bradley, C. A. Efficacy of a PSMA-targeted nanoparticle. *Nat. Rev. Urol.* **2018**, *15*, 590−591.
(10) Duska, L. R.; Krasner, C. N.; O'Malley, D. M.; Hays, J. L.; Modesitt, S. C.; Mathews, C. A.; Moore, K. N.; Thaker, P. H.; Miller, A.; Purdy, C.; Zamboni, W. C.; Lucas, A. T.; Supko, J. G.; Schilder, R. J. A phase Ib/II and pharmacokinetic study of EP0057 (formerly CRLX101) in combination with weekly paclitaxel in patients with recurrent or persistent epithelial ovarian, fallopian tube, or primary peritoneal cancer. *Gynecol. Oncol.* **2021**, *160*, 688−695.
(11) Weiss, G. J.; Chao, J.; Neidhart, J. D.; Ramanathan, R. K.; Bassett, D.; Neidhart, J. A.; Choi, C. H. J.; Chow, W.; Chung, V.; Forman, S. J.; Garmey, E.; Hwang, J.; Kalinoski, D. L.; Koczywas, M.; Longmate, J.; Melton, R. J.; Morgan, R.; Oliver, J.; Peterkin, J. J.; Ryan, J. L.; Schluep, T.; Synold, T. W.; Twardowski, P.; Davis, M. E.; Yen, Y. First-in-human phase 1/2a trial of CRLX101, a cyclodextrin-containing polymer-camptothecin nanopharmaceutical in patients with advanced solid tumor malignancies. *Invest. New Drugs* **2013**, *31*, 986−1000.
(12) Munster, P.; Krop, I. E.; LoRusso, P.; Ma, C.; Siegel, B. A.; Shields, A. F.; Molnár, I.; Wickham, T. J.; Reynolds, J.; Campbell, K.; Hendriks, B. S.; Adiwijaya, B. S.; Geretti, E.; Moyo, V.; Miller, K. D. Safety and pharmacokinetics of MM-302, a HER2-targeted antibody-liposomal doxorubicin conjugate, in patients with advanced HER2-positive breast cancer: a phase 1 dose-escalation study. *Br. J. Cancer* **2018**, *119*, 1086−1093.
(13) Lee, H.; Shields, A. F.; Siegel, B. A.; Miller, K. D.; Krop, I.; Ma, C. X.; LoRusso, P. M.; Munster, P. N.; Campbell, K.; Gaddy, D. F.; Leonard, S. C.; Geretti, E.; Blocker, S. J.; Kirpotin, D. B.; Moyo, V.; Wickham, T. J.; Hendriks, B. S. (64)Cu-MM-302 Positron Emission Tomography Quantifies Variability of Enhanced Permeability and Retention of Nanoparticles in Relation to Treatment Response in Patients with Metastatic Breast Cancer. *Clin. Cancer Res.* **2017**, *23*, 4190−4202.
(14) Steeg, P. S. The blood−tumour barrier in cancer biology and therapy. *Nat. Rev. Clin. Oncol.* **2021**, *18*, 696−714.
(15) Salvioni, L.; Rizzuto, M. A.; Bertolini, J. A.; Pandolfi, L.; Colombo, M.; Prosperi, D. Thirty Years of Cancer Nanomedicine: Success, Frustration, and Hope. *Cancers (Basel)* **2019**, *11*, 1855−1876.
(16) Stylianopoulos, T.; Jain, R. K. Design considerations for nanotherapeutics in oncology. *Nanomedicine* **2015**, *11*, 1893−907.
(17) Liu, J.; Yu, M.; Zhou, C.; Zheng, J. Renal clearable inorganic nanoparticles: a new frontier of bionanotechnology. *Mater. Today* **2013**, *16*, 477−486.
(18) Luhrs, C. A.; Slomiany, B. L. A human membrane-associated folate binding protein is anchored by a glycosyl-phosphatidylinositol tail. *J. Biol. Chem.* **1989**, *264*, 21446−9.
(19) Cheung, A.; Bax, H. J.; Josephs, D. H.; Ilieva, K. M.; Pellizzari, G.; Opzoomer, J.; Bloomfield, J.; Fittall, M.; Grigoriadis, A.; Figini, M.; Canevari, S.; Spicer, J. F.; Tutt, A. N.; Karagiannis, S. N. Targeting folate receptor alpha for cancer treatment. *Oncotarget* **2016**, *7*, 52553−52574.
(20) Scaranti, M.; Cojocaru, E.; Banerjee, S.; Banerji, U. Exploiting the folate receptor α in oncology. *Nat. Rev. Clin. Oncol.* **2020**, *17*, 349−359.
(21) Dosio, F.; Milla, P.; Cattel, L. EC-145, a folate-targeted Vinca alkaloid conjugate for the potential treatment of folate receptor-expressing cancers. *Curr. Opin. Investig. Drugs* **2010**, *11*, 1424−1433.
(22) Graybill, W. S.; Coleman, R. L. Vintafolide: a novel targeted agent for epithelial ovarian cancer. *Future Oncol.* **2014**, *10*, 541−8.
(23) Moore, K. N.; Borghaei, H.; O'Malley, D. M.; Jeong, W.; Seward, S. M.; Bauer, T. M.; Perez, R. P.; Matulonis, U. A.; Running, K. L.; Zhang, X.; Ponte, J. F.; Ruiz-Soto, R.; Birrer, M. J. Phase 1 dose-escalation study of mirvetuximab soravtansine (IMGN853), a folate receptor α-targeting antibody-drug conjugate, in patients with solid tumors. *Cancer* **2017**, *123*, 3080−3087.
(24) Moore, K. N.; Martin, L. P.; O'Malley, D. M.; Matulonis, U. A.; Konner, J. A.; Perez, R. P.; Bauer, T. M.; Ruiz-Soto, R.; Birrer, M. J. Safety and Activity of Mirvetuximab Soravtansine (IMGN853), a Folate Receptor Alpha-Targeting Antibody-Drug Conjugate, in Platinum-Resistant Ovarian, Fallopian Tube, or Primary Peritoneal Cancer: A Phase I Expansion Study. *J. Clin. Oncol.* **2017**, *35*, 1112−1118.
(25) O'Malley, D. M.; Matulonis, U. A.; Birrer, M. J.; Castro, C. M.; Gilbert, L.; Vergote, I.; Martin, L. P.; Mantia-Smaldone, G. M.; Martin, A. G.; Bratos, R.; Penson, R. T.; Malek, K.; Moore, K. N. Phase Ib study of mirvetuximab soravtansine, a folate receptor alpha (FRα)-targeting antibody-drug conjugate (ADC), in combination with bevacizumab in patients with platinum-resistant ovarian cancer. *Gynecol. Oncol.* **2020**, *157*, 379−385.
(26) Moore, K. N.; Oza, A. M.; Colombo, N.; Oaknin, A.; Scambia, G.; Lorusso, D.; Konecny, G. E.; Banerjee, S.; Murphy, C. G.; Tanyi, J. L.; Hirte, H.; Konner, J. A.; Lim, P. C.; Prasad-Hayes, M.; Monk, B. J.; Pautier, P.; Wang, J.; Berkenblit, A.; Vergote, I.; Birrer, M. J. Phase III, randomized trial of mirvetuximab soravtansine versus chemotherapy in patients with platinum-resistant ovarian cancer: primary analysis of FORWARD I. *Ann. Oncol.* **2021**, *32*, 757−765.
(27) Ma, K.; Mendoza, C.; Hanson, M.; Werner-Zwanziger, U.; Zwanziger, J.; Wiesner, U. Control of Ultrasmall Sub-10 nm Ligand-Functionalized Fluorescent Core−Shell Silica Nanoparticle Growth in Water. *Chem. Mater.* **2015**, *27*, 4119−4133.
(28) Ma, K.; Wiesner, U. Modular and Orthogonal Post-PEGylation Surface Modifications by Insertion Enabling Penta-Functional Ultrasmall Organic-Silica Hybrid Nanoparticles. *Chem. Mater.* **2017**, *29*, 6840−6855.
(29) Keam, S. J. Trastuzumab Deruxtecan: First Approval. *Drugs* **2020**, *80*, 501−508.
(30) Larson, D. R.; Ow, H.; Vishwasrao, H. D.; Heikal, A. A.; Wiesner, U.; Webb, W. W. Silica Nanoparticle Architecture Determines Radiative Properties of Encapsulated Fluorophores. *Chem. Mater.* **2008**, *20*, 2677−2684.
(31) Kohle, F. F. E.; Hinckley, J. A.; Wiesner, U. B. Dye Encapsulation in Fluorescent Core−Shell Silica Nanoparticles as Probed by Fluorescence Correlation Spectroscopy. *J. Phys. Chem. C* **2019**, *123*, 9813−9823.
(32) Gardinier, T. C.; Kohle, F. F. E.; Peerless, J. S.; Ma, K.; Turker, M. Z.; Hinckley, J. A.; Yingling, Y. G.; Wiesner, U. High-Performance Chromatographic Characterization of Surface Chemical Heterogeneities of Fluorescent Organic-Inorganic Hybrid Core-Shell Silica Nanoparticles. *ACS Nano* **2019**, *13*, 1795−1804.

https://doi.org/10.1021/acsnano.2c05342
ACS Nano XXXX, XXX, XXX−XXX

(33) Chen, F.; Ma, K.; Benezra, M.; Zhang, L.; Cheal, S. M.; Phillips, E.; Yoo, B.; Pauliah, M.; Overholtzer, M.; Zanzonico, P.; Sequeira, S.; Gonen, M.; Quinn, T.; Wiesner, U.; Bradbury, M. S. Cancer-Targeting Ultrasmall Silica Nanoparticles for Clinical Translation: Physicochemical Structure and Biological Property Correlations. *Chem. Mater.* **2017**, *29*, 8766−8779.
(34) Chen, F.; Ma, K.; Zhang, L.; Madajewski, B.; Zanzonico, P.; Sequeira, S.; Gonen, M.; Wiesner, U.; Bradbury, M. S. Target-or-Clear Zirconium-89 Labeled Silica Nanoparticles for Enhanced Cancer-Directed Uptake in Melanoma: A Comparison of Radiolabeling Strategies. *Chem. Mater.* **2017**, *29*, 8269−8281.
(35) Chen, F.; Ma, K.; Madajewski, B.; Zhuang, L.; Zhang, L.; Rickert, K.; Marelli, M.; Yoo, B.; Turker, M. Z.; Overholtzer, M.; Quinn, T. P.; Gonen, M.; Zanzonico, P.; Tuesca, A.; Bowen, M. A.; Norton, L.; Subramony, J. A.; Wiesner, U.; Bradbury, M. S. Ultrasmall targeted nanoparticles with engineered antibody fragments for imaging detection of HER2-overexpressing breast cancer. *Nat. Commun.* **2018**, *9*, 4141−4152.
(36) Chen, F.; Zhang, X.; Ma, K.; Madajewski, B.; Benezra, M.; Zhang, L.; Phillips, E.; Turker, M. Z.; Gallazzi, F.; Penate-Medina, O.; Overholtzer, M.; Pauliah, M.; Gonen, M.; Zanzonico, P.; Wiesner, U.; Bradbury, M. S.; Quinn, T. P. Melanocortin-1 Receptor-Targeting Ultrasmall Silica Nanoparticles for Dual-Modality Human Melanoma Imaging. *ACS Appl. Mater. Interfaces* **2018**, *10*, 4379−4393.
(37) Chen, F.; Ma, K.; Zhang, L.; Madajewski, B.; Turker, M. Z.; Gallazzi, F.; Cruickshank, K.; Zhang, X.; Jenjitranant, P.; Touijer, K. A.; Quinn, T. P.; Zanzonico, P.; Wiesner, U.; Bradbury, M. S. Ultrasmall Renally Clearable Silica Nanoparticles Target Prostate Cancer. *ACS Appl. Mater. Interfaces* **2019**, *11*, 43879−43887.
(38) Ab, O.; Whiteman, K. R.; Bartle, L. M.; Sun, X.; Singh, R.; Tavares, D.; LaBelle, A.; Payne, G.; Lutz, R. J.; Pinkas, J.; Goldmacher, V. S.; Chittenden, T.; Lambert, J. M. IMGN853, a Folate Receptor-α (FRα)-Targeting Antibody-Drug Conjugate, Exhibits Potent Targeted Antitumor Activity against FRα-Expressing Tumors. *Mol. Cancer Ther.* **2015**, *14*, 1605−13.
(39) Katt, M. E.; Placone, A. L.; Wong, A. D.; Xu, Z. S.; Searson, P. C. In Vitro Tumor Models: Advantages, Disadvantages, Variables, and Selecting the Right Platform. *Front Bioeng. Biotechnol.* **2016**, *4*, 12.
(40) Murayama, T.; Gotoh, N. Patient-Derived Xenograft Models of Breast Cancer and Their Application. *Cells* **2019**, *8*, 621−638.
(41) Rizzo, G.; Bertotti, A.; Leto, S. M.; Vetrano, S. Patient-derived tumor models: a more suitable tool for pre-clinical studies in colorectal cancer. *J. Exp. Clin. Cancer Res.* **2021**, *40*, 178−196.
(42) Shuford, S.; Wilhelm, C.; Rayner, M.; Elrod, A.; Millard, M.; Mattingly, C.; Lotstein, A.; Smith, A. M.; Guo, Q. J.; O'Donnell, L.; Elder, J.; Puls, L.; Weroha, S. J.; Hou, X.; Zanfagnin, V.; Nick, A.; Stany, M. P.; Maxwell, G. L.; Conrads, T.; Sood, A. K.; Orr, D.; Holmes, L. M.; Gevaert, M.; Crosswell, H. E.; DesRochers, T. M. Prospective Validation of an Ex Vivo, Patient-Derived 3D Spheroid Model for Response Predictions in Newly Diagnosed Ovarian Cancer. *Sci. Rep.* **2019**, *9*, 11153−11166.
(43) Guertin, A. D.; O'Neil, J.; Stoeck, A.; Reddy, J. A.; Cristescu, R.; Haines, B. B.; Hinton, M. C.; Dorton, R.; Bloomfield, A.; Nelson, M.; Vetzel, M.; Lejnine, S.; Nebozhyn, M.; Zhang, T.; Loboda, A.; Picard, K. L.; Schmidt, E. V.; Dussault, I.; Leamon, C. P. High Levels of Expression of P-glycoprotein/Multidrug Resistance Protein Result in Resistance to Vintafolide. *Mol. Cancer Ther.* **2016**, *15*, 1998−2008.
(44) Toffoli, G.; Cernigoi, C.; Russo, A.; Gallo, A.; Bagnoli, M.; Boiocchi, M. Overexpression of folate binding protein in ovarian cancers. *Int. J. Cancer* **1997**, *74*, 193−8.
(45) Oronsky, B.; Ray, C. M.; Spira, A. I.; Trepel, J. B.; Carter, C. A.; Cottrill, H. M. A brief review of the management of platinum-resistant-platinum-refractory ovarian cancer. *Med. Oncol.* **2017**, *34*, 103−110.

https://doi.org/10.1021/acsnano.2c05342
ACS Nano XXXX, XXX, XXX−XXX